doi: 10.1111/j.1365-3121.2005.00615.x

Strain localization in sandstone during embryonic stages of shear-zone evolution

Yoram Katz[1,2] and Ram Weinberger[2]

[1]*Institute of Earth Sciences, Hebrew University of Jerusalem, Jerusalem, Israel;* [2]*Geological Survey of Israel, Jerusalem, Israel*

ABSTRACT

Geometric analysis of nested Riedel structures was used to identify and quantify strain localization processes within faulted Navajo sandstone. The analysis shows systematic deviation from the basic Riedel geometry complying with the Mohr–Coulomb criterion. Using cross-cutting relations amongst deformation bands within the Riedel structures, and comparing the orientations of the deformation bands to theoretical strain calculations, we identify two coupling deformation mechanisms involved in the early stages of shear-zone evolution, namely, granular flow and discrete faulting. Both mechanisms localize during strain accumulation, and the granular flow facilitates considerable change in the initial geometry of the Riedel structures. The analysis demonstrates a systematic sequence, by which new Riedel structures form after a constant amount of shear strain takes place in the sandstone. Analysis further indicates that granular flow is the major deformation mechanism during early stages of shear-zone evolution and discrete faulting is the dominant mechanism during later deformation stages.

Terra Nova, 00, 1–6, 2005

Introduction

Deformation in sandstone may take place by more than one mechanism. Field data, laboratory experiments and theoretical analyses have shown that strain accumulation may involve granular (particulate) flow, enabling relative motion of the grains without their breakage, and cataclasis, the crushing of the grains into finer fragments. Cataclasis may be localized in discrete discontinuities, or distributed within the rock (cataclastic flow). The deformation mechanisms of the sandstone is strongly related to the stress state (Zhang *et al*., 1990; Antonellini *et al*., 1994; Menendez *et al*., 1996), the rock porosity (Rutter and Hadizadeh, 1991; Scott and Nielsen, 1991), the mineralogical composition (Rawling and Goodwin, 2003), the cementation characteristics (Underhill and Woodcock, 1987; Ngwenya *et al*., 2001) and the degree of grain sorting (Antonellini and Pollard, 1995). The grain crushing initiates as the effective pressure reaches a critical value (e.g. Zhang *et al*., 1990; Menendez *et al*., 1996), and is therefore depth depended. Fulljames *et al*. (1997) state that within quartz-rich, porous sandstones, the transition between granular flow and cataclasis typically occurs at burial depths of 500–1000 m. According to Bense *et al*. (2003), these mechanisms may alternate gradually from one to the other and coexist within transitional burial conditions. The coupling of these mechanisms is discussed by Borradaile (1981) and Ahlgren (2001).

Correspondence: Dr Yoram Katz, Institute of Earth Sciences, The Hebrew University, Givat-Ram, Jerusalem 91904, Israel. Tel.: +972 2 531 4273; fax: +972 2 538 0688; e-mail: rami@geos.gsi.gov.il

When stress state and burial conditions enable cataclasis during embryonic stages of shear-zone evolution, cataclasis commonly occurs upon numerous small, segmented discontinuities rather than on a single distinct plane. These cataclastic small faults, termed deformation bands, are typically ~1 mm in width and commonly offset several millimetres. Their formation is closely related to collapse of pore space and a consequent major reduction of porosity and permeability (Aydin, 1978; Antonellini and Aydin, 1994; Davis *et al*., 1999). The deformation bands are frequently arranged in particular geometries known as Riedel structures (Fig. 1). The basic Riedel geometry consists of deformation bands oriented sub-parallel to the shear direction and synthetic to the sense of displacement across the shear-zone. These bands, denoted by R, form right-stepping en-echelon arrays along sinistral shear-zones and left-stepping arrays along dextral shear-zones. Overlapping R-bands are typically connected by antithetic deformation bands, denoted by R′. Being conjugate sets, the R and R′-bands intersect in an acute angle of $\beta = 90 - \phi$ and create an angle of about $\phi/2$ and $90 - \phi/2$ to the general shear-zone direction, respectively, where ϕ is the angle of internal friction (Riedel, 1929; Tchalenko, 1968). Recognized also in fault systems of larger scales within various rock types and geological settings, Riedel structures have been widely studied (e.g. Riedel, 1929; Tchalenko, 1970; Moore, 1979; Jamison and Stearns, 1982; Naylor *et al*., 1986; Mandl, 1987; Antonellini and Aydin, 1995; Arboleya and Engelder, 1995; Davis *et al*., 1999; Ahlgren, 2001; Shipton and Cowie, 2001).

In a previous study (Katz *et al*., 2004) we presented outcrop-scale field observations demonstrating systematic deviations from the basic Riedel geometry within adjacent and nested Riedel structures. Using geometrical features, namely the orientation, spacing, spatial distribution and relative age of the deformation bands within the structures, we suggested a conceptual kinematical model which relates the geometry of nested Riedel structures to progressive accumulation and localization of shear strain. According to the model, evolution of a Riedel structure is dominated by two coexisting mechanisms; discrete, abrupt faulting in the form of conjugate deformation bands, and continuous granular flow sub-parallel to the R-deformation bands, causing simple shear of the entire Riedel structure

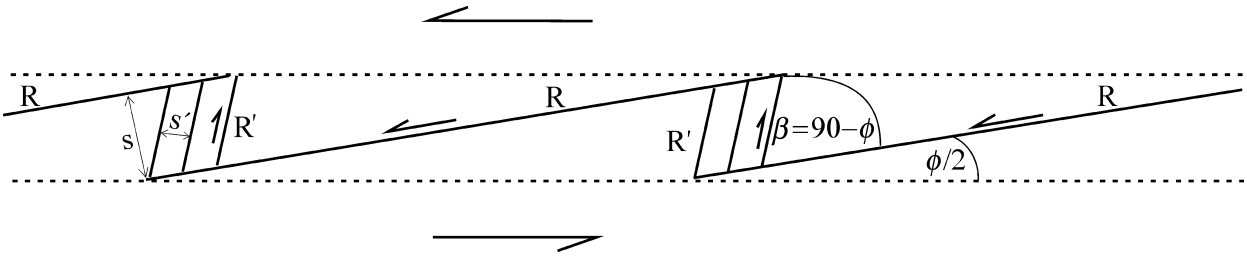

Fig. 1 Basic Riedel shear structures within a sinistral shear-zone. R and R′ are synthetic and antithetic shear bands, respectively, β is the angle between R and R′, s is the R-band spacing, s' is the R′-band spacing and ϕ is the angle of internal friction.

and primary rotation of its R′-deformation bands. The initial angle (β_0) between the R and R′-bands generally complies with the Mohr–Coulomb criterion, exhibiting typical values of 45° (Fig. 2a). As strain accumulates, granular flow across domains bounded by R-bands facilitates rotation and thereby increases the angle β. Upon further strain accumulation, new elongated and narrow Riedel structures are formed, overprinting the older structures (Fig. 2b). Supplementary shear strain is being localized within the new structures, sub-parallel to the general shear direction. Within these domains substantial rotation occurs, changing the primary R′-bands, now rotating as passive markers, into a sigmoidal-like shape (Fig. 2c–d).

In the present study we define quantitatively the relationship between the two deformation mechanisms, using measured angles amongst R′-bands of nested Riedel structures (i.e. Riedel complex). Comparison of these measurements with theoretical strain calculations shows that all R′-bands of a particular Riedel structure are likely to form simultaneously and create a characteristic angle with the R′-bands of earlier formed structures. Moreover, this angle, under minor variance, is common amongst any subsequent R′-band generations. This implies that a constant amount of shear strain, which rotated the R′-bands via granular flow, took place between the creation of any subsequent Riedel generations.

Geologic setting

Field observations were documented in shear zones within the Jurassic Navajo sandstone of Capitol Reef National Park, Utah. The Navajo Formation, underlain by shales and sandstones of the Jurassic Glen-Canyon Group and overlain by shales and sandstones of the Jurassic San Rafael Group, consists of massive, porous, quartz-rich sandstone (Kiersch, 1950; Marzolf, 1983, 1990; Antonellini and Aydin, 1994). This sequence was folded during the formation of the NW–N trending Waterpocket monocline, believed to have initiated at ~75 Ma and to have ceased activity prior to the Eocene (Baker, 1935; Kelley, 1955; Dumitru *et al.*, 1994). The development of the Waterpocket monocline and neighbouring uplifts was associated with regional tectonic deformation that affected the Colorado Plateau of southern Utah during the Laramide (Davis, 1999). The present work was conducted at the northern bank of Capitol Wash, which crosses the monocline from west to east, 6 km south of the Fremont River (Fig. 3).

Using fission-track data, Dumitru *et al.* (1994) constrained the maximum temperature and burial depth of Permian Waterpocket rocks to be ~85–

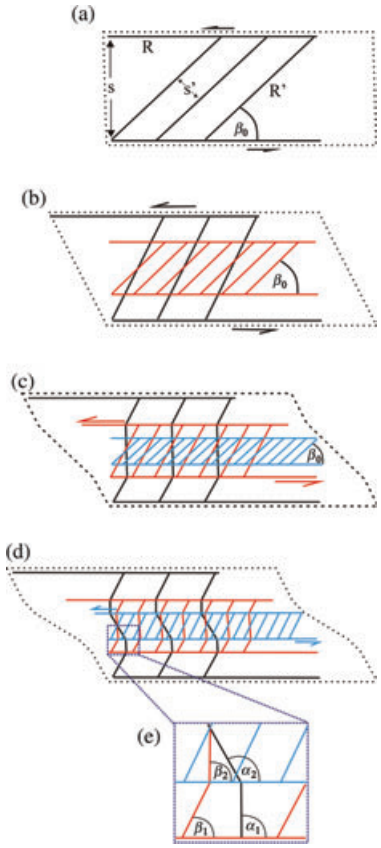

Fig. 2 Computer-derived geometry of nested Riedel structures, demonstrating the evolution of a Riedel complex. In the present case each structure undergoes shear strain of 0.5 before being overprinted by a new structure. The s/s' ratio within each structure is 3, and the overall shear strain (d/s) over the entire complex equals 0.9 by the final stage. (a) Initial, widely distributed Riedel structure characterized by relatively high R and R′-band spacing (black bands). The initial angle between R′-bands and the shear direction is $\beta_0 \approx 45°$. (b) As strain accumulates, granular flow sub-parallel to the R-bands facilitates rotation of the black R′-bands. Upon further strain buildup a second Riedel generation is formed (red bands), creating an angle of $\beta_0 \approx 45°$ with the shear direction and overprinting the older structure. (c) Majority of supplementary strain is localized within the domain enclosed by the second Riedel generation. Strain localization causes pronounced rotation of previous R′-bands bounded by the red R-bands, and further creation of a third Riedel generation (blue bands). (d) Additional localization of strain and rotation within the domain enclosed by the third Riedel generation. (e) Zoom-in showing R′-bands within domains of localized strain. Sectors of the black and red R′-bands create higher angles with the R-band direction (α_2 and β_2, respectively), referred to other sectors within lesser strained domains (α_1 and β_1, respectively).

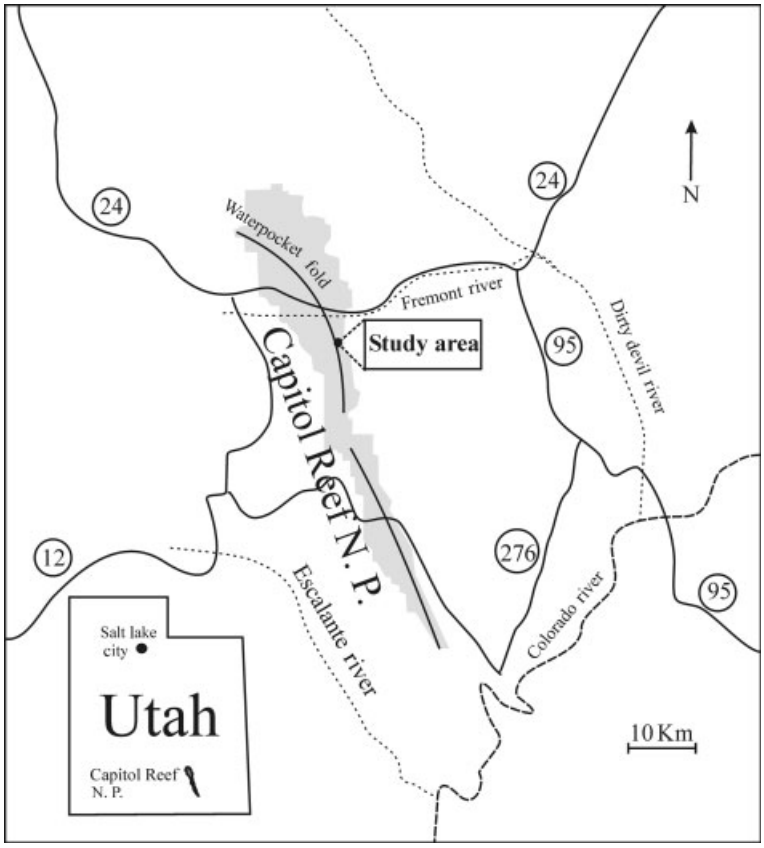

Fig. 3 Location map of Capitol Reef National Park and the study area (after Katz *et al*., 2004).

95 °C and 2–3 km just before the creation of the Waterpocket monocline. This implies maximum temperature and burial depth of ~60 °C and 1–2 km for the overlain Navajo sandstone at that time, assuming normal geothermal gradient.

The stresses associated with the tectonic activity of the Waterpocket monocline, and the burial conditions of the Navajo Formation enabled various internal deformation features to develop in the rock (e.g. Shipton and Cowie, 2001; Bump and Davis, 2003; Davatzes *et al*., 2003). Davis (1999) and Davis *et al*. (1999) documented Riedel structures in conjugate sets at Sheets Gulch, located approximately 16 km south of the present study area, suggesting they accommodated strain during the Laramide regional shortening, perpendicular to the Waterpocket monocline hinge. Roznovsky and Aydin (2001) proposed that major Riedel-structure networks concentrate in areas where the monocline changes its orientation due to underlying fault geometry.

Field observations

Riedel complexes, comprising nested structures of meso to micro scales were documented within sinistral and dextral shear-zones. Figure 4(a) shows such a complex within an E-trending sinistral shear zone. Four generations of Riedel structures were identified using cross-cutting relations; the oldest (generation I) consists of sparse, broadly distributed deformation bands, and is overprinted by a more localized, denser structure (generation II). Generations I and II are overprinted by a younger structure, exhibiting a dense network of deformation bands and restricted to narrow and elongated domains (generation III). A few R′-bands which belong to a fourth generation overprint all former structures. The en-echelon architecture of the R-bands is apparent within the structures of generations II and III.

Orientation of R′-bands were measured within an exposure of detailed nested Riedel structures (Fig. 4b). Noticeably, R′-bands of the same generation appear to be sub-parallel.

Shear strain and line rotation

Our kinematical model is based on the geometrical relations between the simple shear strain imposed on a material and the consequent rotation of a line within it. This is expressed as (after Ramsay and Huber, 1983):

$$\gamma = \frac{\sin(\beta_2 - \beta_1)}{\sin\beta_1 \sin\beta_2}, \qquad (1)$$

where γ is the shear strain, β_1 and β_2 are the angles between the line and the shear direction before and after rotation, respectively, and $(\beta_2 - \beta_1)$ is referred to as the line rotation angle (Fig. 5).

Using Eq. (1) and given the orientation of any pair of lines in the material prior to shearing, new orientations of the lines can be calculated as a function of the imposed shear strain. The orientation of such a pair can be demonstrated by a single point (β_i,α_i) on a graph, henceforth denoted as a line rotation diagram (Fig. 5c). Of the two angles created between the lines of the pair and the shear direction, β represents the smaller angle and α represents the larger one. Among further shear and consequent rotation of the lines, the point (β_i,α_i) follows a unique curved path which depends solely on the initial orientation of the lines.

During the formation of nested Riedel structures, new structures overprint previous ones and R′-bands of younger generations cross-cut older R′-bands. Due to varying degrees of shear within different locations in the complex, different sectors of a pair of cross-cutting R′-bands may undergo different amounts of rotation (Fig. 2e). Based on the principle presented in Fig. 5(c), when drawn on a line rotation diagram, the points representing different sectors of the pair will align along the same unique curve, depending solely on the initial orientation of the pair.

This principle may gain wider significance if two conditions are met during the formation of any Riedel structure within the complex: first, if all R′-bands of a particular structure are formed simultaneously, and second, if they share a common orienta-

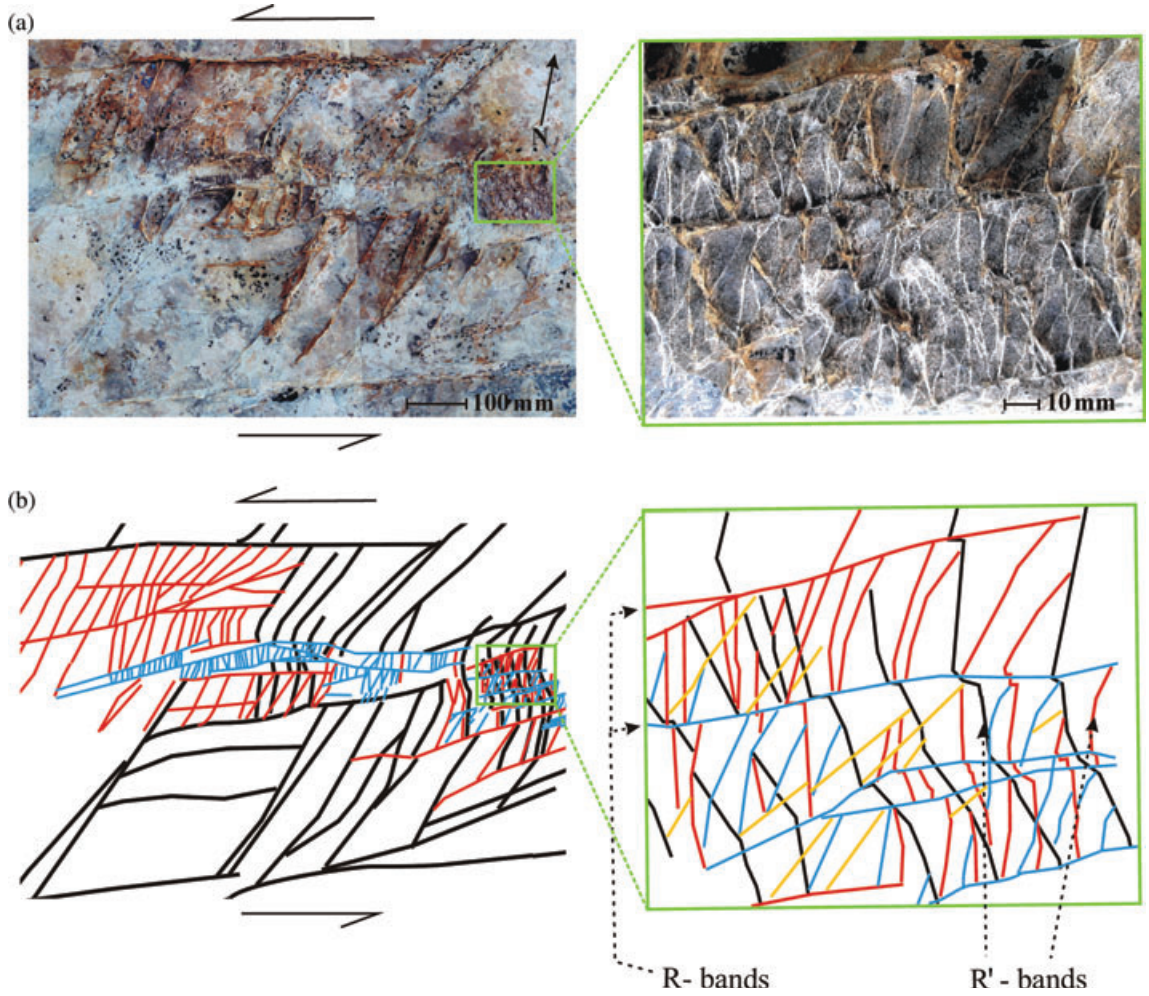

Fig. 4 (a) Nested Riedel structures within an E-trending sinistral shear zone. Inset shows details of angular and cross-cutting relations between R′-bands of different generations. (b) Drawings of the deformation bands shown in (a). Four generations of Riedel structures were identified using cross-cutting relations; black (oldest, denoted 'Generation I' in text), red (denoted 'Generation II'), blue (denoted 'Generation III'), and yellow (youngest, denoted 'Generation IV').

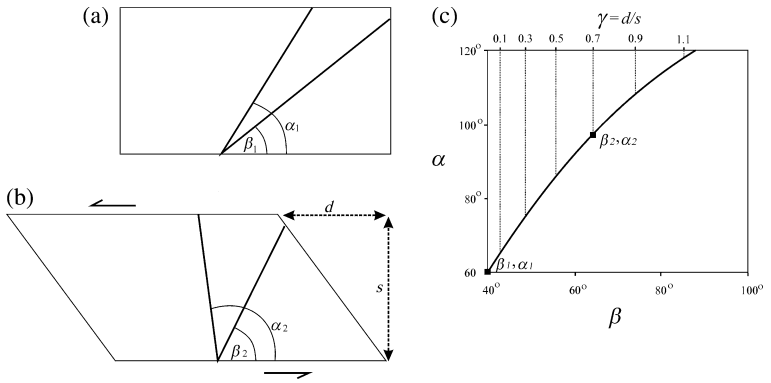

Fig. 5 Orientation of a pair of lines within a material: (a) before simple shear takes place, and (b) after simple shear ($\gamma = d/s = 0.7$) takes place. (c) Orientation of the pair is demonstrated by a line rotation diagram, showing its initial (β_1,α_1) and final (β_2,α_2) positions as a function of shear strain γ. During rotation of the pair, the point (β_i,α_i) follows a unique curved path which depends solely on the initial position of the pair.

tion as they form. If these two conditions are satisfied, the orientation of all pairs composed by R′-bands of two given subsequent generations must be initially similar. Consequently, all pairs composed of subsequent generations must be represented by points that align along the same unique curve on the line rotation diagram, regardless of their location within the complex and the amount of strain they were subjected to.

The measurements for pairs composed of subsequent R′-band generations are presented and compared to theoretical orientation curves in Fig. 6. β and α values represent the angles that the younger and older R′-band of each pair create with the shear direction, respectively. It is apparent

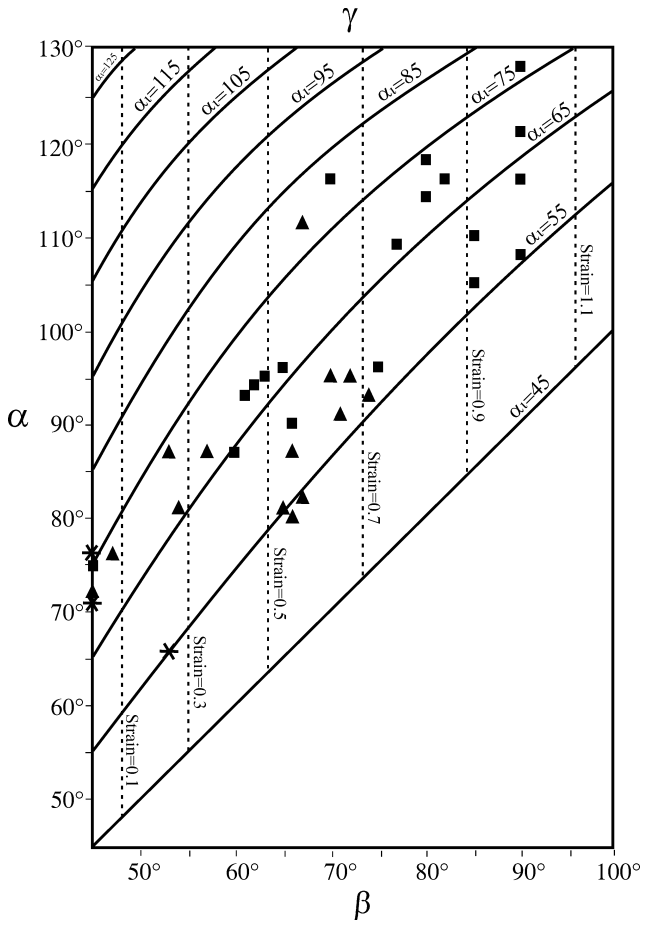

Fig. 6 Measured orientations of R′-bands, presented on a line rotation diagram. Rectangles represent pairs of R′-bands composed of generations I and II, triangles represent pairs composed of generations II and III and stars represent pairs composed of generations III and IV. β and α values correspond to the orientations of the younger and older R′-band within each pair, respectively. Solid curves provide calculated orientations as a function of the shear strain γ and various initial pair orientations. Each curve is calculated assuming the younger R′-band is initially oriented 45° to shear direction, and the older R′-band is oriented to a higher angle, indicated on the curve as α_i. The dashed, vertical lines represent the amount of shear strain to which a pair was subjected since the younger R′-band formed. As different sectors of the same pair may rotate to a different degree (see Fig. 2e), the results are scattered. Yet, the older pairs (rectangles) generally exhibit intermediate to high angles and the younger pairs (triangles) exhibit intermediate to low angles. The youngest pairs (stars), only scarcely sheared, exhibit especially low angles.

that the majority of the measurements (29 of 35) align within the curve calculated for initial $(\beta,\alpha) = (45°, 55°)$, and the curve calculated for initial $(\beta,\alpha) = (45°, 75°)$.

Discussion and conclusions

The observations exhibit two main features that should be highlighted. The first is the sub-parallelism of R′-bands that belong to the same Riedel structure, and underwent the same amount of shear strain. This indicates that the R′-bands were formed simultaneously and shared the same initial orientation. As shown by Katz *et al.* (2004) for the Navajo sandstone, the initial angle β_0 between the R′-bands and R-band's direction generally complies with the Mohr–Coulomb criterion, exhibiting typical values of 45°. The second is the alignment of over 80% of the measurements within the curve calculated for initial $(\beta,\alpha) = (45°, 55°)$ and the curve calculated for initial $(\beta,\alpha) = (45°, 75°)$, implying a particular evolution of the band's orientation with shear. These measurements suggest that within any pair of subsequent R′-bands, the former R′-band had already been rotated to 65 ± 10°, with respect to the R-band direction, by the time the latter R′-band formed, orienting about 45° with respect to the same reference. Accordingly, the deformed Navajo sandstone underwent simple shear strain of approximately 0.5 ± 0.2 via granular flow, between each formation of a new Riedel structure.

Given this relationship between the two coexisting mechanisms, and given the limited offset of up to several millimetres on a single deformation band (Aydin, 1978), it is important to quantify the relative contribution of each mechanism to the overall rock deformation. As shear strain (d/s) that occurs between faulting episodes is roughly constant, d values are in accordance with the values of s. Hence, during the early stages of the Riedel complex evolution, as structures are sparse and spacing s between R-bands is large, d values are high and only a few subsequent Riedel generations are formed during a given slip on the Riedel complex. At later stages however, when deformation localizes to narrow domains and R-band spacing becomes small, low d values enable more discrete faulting episodes to take place during a given slip on the complex. It is therefore suggested that at early stages of the Riedel complex evolution the granular flow is the dominant deformation mechanism, whereas at later stages the discrete faulting overrides and becomes the dominating one. This conclusion is in accordance with field observations, showing the latest Riedel structure domains to be comprised almost entirely of faulted and crushed quartz grains.

We have been able to uncover the nature and characterize the relationship between two deformation mechanisms which govern the embryonic stages of shear zone evolution in sandstone. The question still remains, however, what causes the coexistence of these two different mechanisms under the same stress conditions. Realizing the relationship between them, we suggest that stresses which are accommodated during shear via

granular flow are released during the episodes of discrete faulting. Depending on the mechanical properties of the rock, the faulting will take place at every given amount of shear strain, which averages 0.5 in the Navajo sandstone.

Acknowledgements

This study was supported by grant no. 9800198 from the United State-Israel Binational Science Foundation (BSF). We are indebted to A. Aydin for introducing us with the study area and for stimulating discussions during the course of this study. We benefited from fruitful discussions with V. Lyakhovsky and A. Starinsky.

References

Ahlgren, S.G., 2001. The nucleation and evolution of Riedel shear-zones as deformation bands in porous sandstone. *J. Struct. Geol.*, **23**, 1203–1214.

Antonellini, M.A. and Aydin, A., 1994. Effects of faulting on fluid flow in porous sandstones: petrophysical properties. *Am. Assoc. Petrol. Geol. Bull.*, **78**, 355–377.

Antonellini, M.A. and Aydin, A., 1995. Effects of faulting on fluid flow in porous sandstones: geometry and spatial distribution. *Am. Assoc. Petrol. Geol. Bull.*, **79**, 642–671.

Antonellini, M.A. and Pollard, D.D., 1995. Distinct element modeling of deformation bands in sandstone. *J. Struct. Geol.* **17**, 1165–1182.

Antonellini, M.A., Aydin, A. and Pollard, D.D., 1994. Microstructures of deformation bands in porous sandstones at Arches National Park, Utah. *J. Struct. Geol.*, **16**, 941–959.

Arboleya, M.L. and Engelder, T., 1995. Concentrated slip zones with subsidiary shears: their development on three scales in the Cerro Brass fault zone, Appalachian valley and ridge. *J. Struct. Geol.*, **17**, 519–532.

Aydin, A., 1978. Small faults formed as deformation bands in sandstones. *Pure Appl. Geophys.*, **116**, 913–930.

Baker, A.A., 1935. Geologic structure of southeastern Utah. *Am. Assoc. Petrol. Geol. Bull.*, **19**, 1472–1507.

Bense, V.F., Van den Berg, E.H. and Van Balen, R.T., 2003. Deformation mechanisms and hydraulic properties of fault zones in unconsolidated sediments; the Roer Valley Rift System, The Netherlands. *Hydrogeol. J.*, **11**, 319–332.

Borradaile, G.J., 1981. Particulate flow of rock and formation of cleavage. *Tectonophysics*, **72**, 305–321.

Bump, A.P. and Davis G.H., 2003. Late Cretaceous–early Tertiary Laramide deformation of the northern Colorado Plateau, Utah and Colorado. *J. Struct. Geol.*, **25**, 421–440.

Davatzes, N.C., Aydin, A. and Eichhubl, P., 2003. Overprinting faulting mechanisms during the development of multiple fault sets in sandstone, Chimney Rock fault array, Utah, USA. *Tectonophysics*, **363**, 1–18.

Davis, G.H., 1999. Structural geology of the Colorado Plateau region of southern Utah, with special emphasis on deformation bands. *Geol. Soc. Am. Spec. Pap.*, **342**, 157.

Davis, G.H., Bump, A.P., Garcia, P.E. and Ahlgren, S.G., 1999. Conjugate Riedel deformation band shear-zones. *J. Struct. Geol.*, **22**, 169–190.

Dumitru, T.A., Duddy, I.A. and Green, P. F., 1994. Mesozoic-Cenozoic burial, uplift and erosion history of the west-central Colorado Plateau. *Geology*, **22**, 499–502.

Fulljames, J.R., Zijerveld, J.J. and Franssen, R.C.M.W., 1997. Fault seal processes: systematic analysis of fault seals over geological and production time scales. In: *Hydrocarbon Seals – Importance for Exploration and Production* (P.K. Møller-Pedersen and A.G. Koestler, eds). *Norw. Petrol. Soc. NPF Spec. Publ.*, **7**, 51–59.

Jamison, W.R. and Stearns, D.W., 1982. Tectonic deformation of Wingate sandstone, Colorado National Monument. *Am. Assoc. Petrol. Geol. Bull.*, **66**, 2584–2608.

Katz, Y., Weinberger, R. and Aydin, A., 2004. Geometry and kinematic evolution of Riedel shear structures, Capitol Reef National Park, Utah. *J. Struct. Geol.*, **26**, 491–501.

Kelley, V.C., 1955. Monoclines of the Colorado Plateau. *Geol. Soc. Am. Bull.*, **66**, 789–803.

Kiersch, G.A., 1950. Small-scale structures and other features of Navajo Sandstone, northern part of the San-Rafael Swell, Utah. *Am. Assoc. Petrol. Geol. Bull.*, **34**, 923–942.

Mandl, G., 1987. Tectonic deformation by rotating parallel faults: the "bookshelf" mechanism. *Tectonophysics*, **141**, 277–316.

Marzolf, J.E., 1983. Changing winds and hydraulic regimes during deposition of the Navajo and Aztec sandstones, Jurassic (?) southwestern United States. In: *Eolian Sediments and Processes* (M.E. Brookfield and T.S. Ahlbrandt, eds), pp. 635–660. Elsevier, Amsterdam.

Marzolf, J.E., 1990. Reconstruction of extensionally dismembered early Mesozoic sedimentary basins; southwestern Colorado Plateau to the eastern Mojave Desert. In: *Basin and Range Extensional Tectonics Near the Latitude of Las Vegas, Nevada* (B.P. Wernicke, ed.), *Geol. Soc. Am. Mem.*, **176**, 477–500.

Menendez, B., Zhu, W. and Wong, T.-F., 1996. Micromechanics of brittle faulting and cataclastic flow in Berea sandstone. *J. Struct. Geol.*, **18**, 1–16.

Moore, J.M., 1979. Tectonics of the Najad transcurrent fault system, Saudi Arabia. *J. Geol. Soc. London*, **136**, 441–452.

Naylor, M.A., Mandl, G. and Sijpesteijn, C.H.K., 1986. Fault geometries in basement-induced wrench faulting under different initial stress states. *J. Struct. Geol.*, **8**, 737–752.

Ngwenya, B.T., Main, I.G., Elphick, S.C., Crawford, B.R. and Smart, B.G.D., 2001. A constitutive law for low-temperature creep of water-saturated sandstones. *J. Geophys. Res.*, **106**, 21811–21826.

Ramsay, J.G. and Huber, M.I., 1983. *The Techniques of Modern Structural Geology. Volume 1: Strain Analysis.* Academic Press, London.

Rawling, G.C. and Goodwin, L.B., 2003. Cataclasis and particulate flow in faulted, poorly lithified sediments. *J. Struct. Geol.*, **25**, 317–331.

Riedel, W., 1929. Zur Mechanik Geologischer Brucherscheinungen. *Zbl. Mineral. Geol. Paleontol. B*, 354–368.

Roznovsky, T.A. and Aydin, A., 2001. Concentration of shearing deformation related to changes in strike of monoclinal fold axes: the Waterpocket monocline, Utah. *J. Struct. Geol.*, **23**, 1567–1579.

Rutter, E.H. and Hadizadeh, J., 1991. On the influence of porosity on the low-temperature brittle-ductile transition in siliciclastic rocks. *J. Struct. Geol.*, **13**, 609–614.

Scott, T.E. and Nielsen, K.C., 1991. The effects of porosity on the brittle-ductile transition in sandstones. *J. Geophys. Res.*, **96**, 405–414.

Shipton, Z.K. and Cowie, P.A., 2001. Damage zone and slip-surface evolution over μm to km scales in high-porosity Navajo sandstone, Utah. *J. Struct. Geol.*, **23**, 1825–1844.

Tchalenko, J.S., 1968. The evolution of kink-bands and the development of compression textures in sheared clays. *Tectonophysics*, **6**, 159–174.

Tchalenko, J.S., 1970. Similarities between shear-zones of different magnitudes. *Geol. Soc. Am. Bull.*, **81**, 1625–1640.

Underhill, J.R. and Woodcock, N.H., 1987. Faulting mechanism in high-porosity sandstones; New Red Sandstone, Arran, Scotland. In: *Deformation of Sediments and Sedimentary Rocks* (M.E. Jones and R.M.F. Prestone, eds). *Geol. Soc. London Spec. Publ.*, **29**, 91–105.

Zhang, J., Wong, T.-F. and Davis, D.M., 1990. Micromechanics of pressure-induced grain crushing in porous rocks. *J. Geophys. Res.*, **95**, 341–352.

Received 8 July 2004; revised version accepted 18 January 2005

